Materials Today Bio 28 (2024) 101208

Contents lists available at ScienceDirect

Materials Today Bio

journal homepage: www.journals.elsevier.com/materials-today-bio

Enhancing long-segmental tracheal restoration: A self-repairing hydrogel loaded with chondrocytokines for sutureless anastomosis and cartilage regeneration

Liang Guo [a,1], Xuezhe Liu [b,1], Yao Wang [a,1], Jiaoyu Yi [c], Juanjuan Li [e], Yong Xu [a], Kaiyong Cai [b], Wufei Dai [d,**], Qian Feng [b,*], Bo Tao [a,***]

[a] Department of Thoracic Surgery, Shanghai Pulmonary Hospital, Tongji University School of Medicine, Shanghai, China
[b] Key Laboratory of Biorheological Science and Technology, Ministry of Education, College of Bioengineering, Chongqing University, Chongqing, China
[c] Department of Plastic Surgery, Renji Hospital, Shanghai Jiao Tong University, School of Medicine, Shanghai, China
[d] Department of Plastic and Reconstructive Surgery, Shanghai 9th People's Hospital, Shanghai Jiao Tong University School of Medicine, Shanghai, China
[e] Department of Medical Oncology, Shanghai Pulmonary Hospital and Thoracic Cancer Institute, Tongji University School of Medicine, Shanghai, China

ARTICLE INFO

Keywords:
Hydrogel
Suture-free
Self-healing
Tracheal reconstruction
Dual-drug encapsulation

ABSTRACT

Artificial tracheal substitutes encounter significant challenges during long-segmental tracheal defects (LSTD) reconstruction, notably early postoperative anastomotic stenosis and tracheal chondromalacia. Mitigating early anastomotic stenosis by creating a compliant sutureless substitute is pivotal. Enhancing its chondrogenic capacity is equally critical for sustained healthy tracheal cartilage regeneration. This study proposes a self-healing hydrogel for sutureless tracheal anastomosis to mitigate anastomotic stenosis, enriched with kartogenin (KGN) and transforming growth factor-β1 (TGFβ1) to bolster chondrogenic properties. Initially, two precursor solutions were prepared: 1) aldehyde-modified hyaluronic acid with sulfonation and β-cyclodextrin-CHO loaded with KGN; 2) hydrazide-grafted gelatin loaded with TGFβ1. Coextrusion of these solutions resulted in a gelated G + TGFβ1/sH-CD + KGN hydrogel, characterized by a robust covalent bonding network of acylhydrazones between hydrazide and aldehyde groups, imparting excellent self-healing properties. The G + TGFβ1/sH-CD + KGN hydrogels, showcasing favorable cytocompatibility, excellent injectability, and rapid gelation, were loaded with bone marrow stem cells. These were customized into O-shaped rings and assembled into a malleable tracheal substitute using our established ring-to-tube method. This resultant compliant substitute facilitated sutureless anastomosis of LSTD in a rabbit model, attributed to the Schiff base reaction between the hydrogel's carbonyl group and the tissue's amino group. Notably, the tracheal substitute reduced early postoperative anastomotic stenosis, maintained tracheal patency, alleviated sputum blockage, promoted reepithelization, and increased the survival rate of the experimental rabbits. The sustained release of chondrocytokines resulted in excellent tracheal cartilage regeneration. Employing chondrocytokines-loaded hydrogels with self-healing properties represents a significant advancement in sutureless tracheal anastomosis and tracheal cartilage regeneration, holding promising potential in inhibiting early postoperative anastomotic stenosis and tracheal chondromalacia when treating LSTD.

1. Introduction

Over the last century, thoracic surgery has evolved, rendering the trachea accessible for surgical interventions. Surgical resection and reconstruction have gradually superseded endoscopic treatments, becoming the favored approach for diverse tracheal diseases. However, surgeries for long-segment tracheal defects (LSTD) necessitate advanced skills and often demand multidisciplinary collaboration, limiting their

* Corresponding author.
** Corresponding author.
*** Corresponding author.
E-mail addresses: daiwfup@163.com (W. Dai), qianfeng@cqu.edu.cn (Q. Feng), tbo0820@163.com (B. Tao).
[1] These authors contributed equal to this work.

https://doi.org/10.1016/j.mtbio.2024.101208
Received 31 December 2023; Received in revised form 17 August 2024; Accepted 23 August 2024
Available online 30 August 2024

execution to select tertiary care centers. Despite these advancements, patients encounter various postoperative complications, and the viable resectable length of the trachea remains limited. In cases where the affected area surpasses specific thresholds—50 % in adults or 30 % in children—primary surgical anastomosis becomes unfeasible due to excessive tension [1]. Consequently, attention has shifted towards exploring tracheal substitutes to address LSTD. Yet, existing substitutes fall short of yielding ideal therapeutic outcomes.

Currently, various tracheal substitution protocols have been attempted for clinical application, including autologous tissue transplants [2,3], allografts [4,5], and bioprosthetic implants [6,7], which achieving some initial promising results. However, due to the extreme technical difficulty, the unstable donor sources, and the need for long-term immunosuppression, these methods cannot be generalized promoted in clinical practice at this stage. More critically, due to the lack of natural bionic tracheal structure and mechanical properties, long-term lumen patency could only be achieved in a minority of tracheal substitutes.

Fortunately, biomaterial-based tracheal substitutes, which consist of a material skeleton and few proliferating autologous cells, addressed the drawbacks of poor mechanical properties of autologous substitutes and the poor biocompatibility of allogeneic substitutes at one stroke. For its tunable mechanical strength and ability to be individually tailored, biomaterial-based tracheal substitutes have received extensive attention in academia. Through previous research, our team discovered that regenerating cartilaginous rings with a layered structure can mimic the natural tracheal structure and mechanical properties, improving the effectiveness of tracheal reconstruction [8]. Although favorable early reconstructive results were achieved, long-term tracheal patency still faces many problems, among which anastomotic stenosis, which occurs in the early postoperative period, is the main obstacle to long-term patency after tracheal reconstruction for this stage.

Studies indicate that poor compliance of tracheal substitutes might be a primary cause leading to re-stenosis at the anastomotic site [9,10]. It is well known that rigidity is an essential property to maintain tracheal patency, most materials can easily achieve the lateral stiffness well beyond the strength of the trachea. However, solely pursuing reliable rigid support creates a significant difference in stress between the graft and the autologous trachea. Stiff materials, in between breaths, cause friction with autologous tissue, leading to inflammatory edema at the anastomotic site, fundamentally contributing to severe early postoperative granulation tissue hyperplasia. Hence, enhancing the early mechanical compliance of tracheal substitutes to eliminate stress on autologous tissue is crucial for reducing inflammatory reactions at the anastomotic site and preventing early stenosis post-surgery.

Furthermore, surgical sutures contribute significantly to re-stenosis at the anastomotic site. Though the widespread use of absorbable sutures has substantially reduced inflammatory reactions in the body, commonly used sutures like polyglactin and polydioxanone require at least 6–8 months to degrade [11], overlapping with the postoperative inflammatory response period. This inevitably intensifies the aggregation of inflammatory cells at the anastomotic site, aggravating granulation growth. Additionally, tight suture lines affect the blood supply and endothelial cell migration near the anastomotic site, hindering vascularization and endothelialization of the tracheal substitute [12]. Thus, designing a sutureless and highly compliant tracheal substitute is expected to reduce re-stenosis at the anastomotic site post-transplantation, achieving long-term tracheal patency.

Injectable hydrogel materials, with their strong plasticity, controllable mechanical properties, and tissue adhesion characteristics, have been proven suitable for repairing different parts of the human body. Leveraging the favorable plasticity and innate softness of injectable hydrogels allows the production of ring-shaped tracheal substitutes with excellent mechanical compliance and diverse sizes. By the active modification of the skeleton material, hydrogels can be endowed with self-healing capabilities, while also greatly improving adhesion to biological surfaces, which in turn reduces or eliminates the use of surgical sutures.

In light of these considerations, our aim is to create a compliant and sutureless tracheal substitute with robust chondrogenic capabilities, targeting the early postoperative prevention of anastomotic re-stenosis and tracheal chondromalacia. To achieve this, we initiated the process by synthesizing aldehyde-modified hyaluronic acid with sulfonation (HA-CHO-SO_3) and hydrazide-grafted gelatin (gelatin-ADH). The coextrusion of these compounds triggers a condensation reaction between their hydrazide and aldehyde groups, forming a network of acylhydrazones, imparting exceptional self-healing properties. Moreover, the interaction between the hydrogels' carbonyl group and the native tissue's amino group facilitates remarkable tissue adhesion. Following this, we incorporated the chondrogenic cytokine TGFβ1 into the hydrogel via HA-CHO-SO_3, exploiting the electrostatic interactions between the positively charged amino acid residues of TGFβ1 and the negatively charged sulfated groups of the HA skeleton. Simultaneously, another chondrogenic cytokine, KGN, was captured by synthesized β-cyclodextrin-CHO (β-CD-CHO) through a host-guest interaction between β-CD and KGN. By combining KGN-loaded β-CD-CHO with the aforementioned hydrogel, KGN was successfully linked to the gelatin skeleton via a condensation reaction. Subsequently, the dual chondrogenic cytokines-loaded self-healing hydrogel (G + TGFβ1/sH-CD + KGN) was created by coextruding solution 1 (HA-CHO-SO_3, β-CD-CHO, and KGN) and solution 2 (gelatin-ADH and TGFβ1) using a double-barreled syringe. Additionally, bone marrow stem cells (BMSCs) were loaded into the G + TGFβ1/sH-CD + KGN hydrogel and injected into O-shaped rings for both *in vitro* and *in vivo* chondrogenesis evaluations. Finally, these O-shaped hydrogel rings were assembled into flexible tracheal substitutes using the ring-to-tube method. These substitutes were utilized for repairing LSTD via sutureless anastomosis in rabbits (Scheme 1). Our ultimate goal is to inhibit early postoperative anastomotic stenosis and tracheal chondromalacia through this innovative approach.

2. Materials and methods

2.1. Preparation of hydrogels

2.1.1. Preparation of HA-CHO-SO_3

First, dissolve 2 g of hyaluronic acid (HA, MW = 100 kDa, Focus-Freda, China) in 200 mL of deionized water. Then add 1.2 g of sodium periodate ($NaIO_4$, AR, Macklin, China) in dark, reacting 24 h at room temperature. Following the method described previously [13], purify the aldehyde-modified hyaluronic acid (HA-CHO) through dialysis.

Take 1 g of the purified HA-CHO dissolved in 100 mL of deionized water. Add 3 g of anion exchange resin (Dowex®50W 200) and stir at room temperature for 8 h. Adjust the pH of the solution to 7.02–7.05 using tetra propyl ammonium hydroxide (TPAOH, Sigma, USA). After freeze-drying, obtain HA-CHO-TPA.

Dissolve 0.35 g of HA-CHO-TPA in 70 mL of N,N-Dimethylformamide (DMF, Macklin, China). After complete dissolution, add 7 mL of a 9 % (W/V) solution of sulfur trioxide pyridine (SO_3-pyridine, Sigma, USA) in DMF under nitrogen atmosphere, reacting 20 min at room temperature. Dialyze the resulting mixture in NaCl solution for 2 days and then in deionized water for 3 days. Finally, vacuum dry to obtain HA-CHO-SO_3. The sulfur content in the product was determined using an elemental analyzer (Vario EL Cube, Germany) via microcombustion. The formula for calculating the content of sulfated groups was obtained by dividing the measured percentage of sulfur content by the relative molecular mass of sulfur, resulting in the mole number of sulfated group per gram of sample.

The reaction of tert-butyl carbazone (t-BC) with the aldehyde groups of HA-CHO and a reference substance was conducted as follows: Initially, a series of standard samples with concentrations ranging from 5 to 30 × 10^3 M were prepared to generate a calibration curve for absorbance measurements. Subsequently, a mixture was prepared by

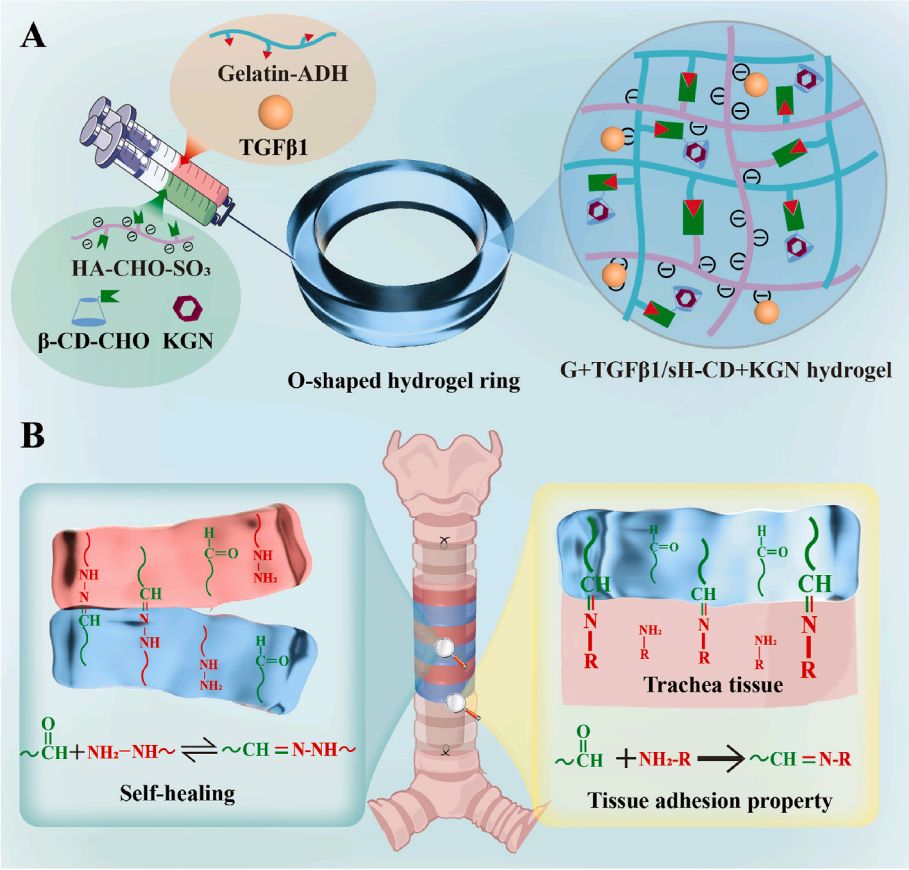

Scheme 1. Development and application of G + TGFβ1/sH-CD + KGN. (A) Initially, two solutions were prepared: one composed of HA-CHO-SO_3 and β-CD-CHO loaded with KGN, while the other contained gelatin-ADH loaded with TGFβ1. These solutions were coextruded through a double-barreled syringe, forming ring-shaped hydrogels that were injected into O-shaped molds. The resulting gelated G + TGFβ1/sH-CD + KGN hydrogel demonstrated excellent self-healing properties due to the network of acylhydrazones formed between the hydrazide and aldehyde groups in the side chain. KGN was loaded onto β-CD-CHO and linked to the gelatin skeleton through a condensation reaction. TGFβ1 was captured through electrostatic interactions with the -SO3 group introduced in the HA skeleton. (B) Leveraging the self-healing characteristics, both BMSCs loaded and unloaded hydrogels in O-shape were arranged alternately using our previously established ring-to-tube method to create a tracheal substitute. The G + TGFβ1/sH-CD + KGN hydrogel exhibited excellent tissue adhesive properties due to the Schiff base reaction between the hydrogel's carbonyl group and the native tissue's amino group. These tracheal substitutes were utilized for sutureless anastomosis to repair LSTD in a rabbit model.

combining 25 μL of 0.6 % w/v HA-CHO solution with an equal volume of 30×10^3 M t-BC solution in 1 % w/v trichloroacetic acid solution. This mixture was allowed to react at room temperature. After 24 h of incubation, a solution of 2,4,6-trinitrobenzenesulfonic acid (TNBS) (0.5 mL, 6×10^3 M in 0.1 M borate buffer) was added to the mixture to react with any unreacted t-BC for 1 h. Post-reaction, a 50 μL aliquot from the reaction mixture was diluted with 150 μL of 0.5 M HA. The absorbance of the resulting solution was measured at a wavelength of 340 nm using a spectrophotometer, with each sample tested in triplicate to ensure accuracy and reproducibility.

2.1.2. Preparation of β-cd-cho

Dissolve 0.2 g of β-cyclodextrin (β-CD, Sigma, USA) and 0.14 g of Dess-Martin periodinane (DMP, Macklin, China) in 5 mL of DMF, and the mixture was stirred for 1 h at 25 °C. Then cool the mixture overnight at −20 °C to obtain crude aldehyde-modified β-cyclodextrin (β-CD-CHO). Purify the crude product by dropping it into 150 mL of cold acetone to remove unreacted DMP and β-CD. Precipitate and centrifuge the product at least 3 times. Finally, obtain pure β-CD-CHO through vacuum drying.

2.1.3. Preparation of Gelatin-ADH

Dissolve 2 g of gelatin (A type, Sigma, USA) in 200 mL of 4-Morpholineethanesonic acid (MES, Macklin, China) buffer solution (pH = 6.5). Slowly add 2.5 g of N-(3-Dimethylaminopropyl)-N′-ethylcarbodiimide hydrochloride (EDC, Macklin, China) and 1.78 g of 1-hydroxy-benzotriazole (HOBT, J&K Scientific, China) to activate the carboxyl groups in gelatin. After stirring for 1 h, add 9 g of adipic acid dihydrazide (ADH, Macklin, China). After 24 h of reaction, obtain crude ADH-modified gelatin (gelatin-ADH). Finally, use dialysis and vacuum drying of the crude product to obtain gelatin-ADH.

2.1.4. Preparation of G/H, G/sH-cd, G/sH-cd + KGN, G + TGFβ1/sH-cd, G + TGFβ1/sH-cd + KGN hydrogels

Dissolve gelatin-ADH and HA-CHO separately in phosphate buffered saline (PBS, Sigma, USA). Mix the two solutions in a 1:1 vol ratio using a double-barreled syringe to obtain G/H hydrogel. By adjusting the concentrations of gelatin-ADH (x% = 8 %, 10 %, 12 %, 14 %, 16 %, 18 %) and HA-CHO (y% = 2 %, 4 %), obtain Gx/Hy hydrogels.

Prepare the G + TGFβ1 solution (referred to as solution 1) by loading 200 ng/mL TGFβ1 into gelatin-ADH. Prepare the sH-CD + KGN solution (referred to as solution 2) by loading 50 μM KGN into HA-CHO-SO_3/β-CD-CHO. Finally, coextrude solutions 1 and 2 in a 1:1 vol ratio to obtain the G + TGFβ1/sH-CD + KGN hydrogel. The hydrogels G/sH, G/H-CD, G/sH-CD, G/sH-CD + KGN, and G + TGFβ1/sH-CD were prepared using the same coextrusion method. The detailed compositions of solutions 1 and 2 are listed in Table S1 (**Supplemental Information**).

2.2. Characterization of hydrogels

2.2.1. Fourier Transform Infrared Spectroscopy

The purified and dried polymer or small molecule sample and an appropriate amount of dried potassium bromide powder were thoroughly ground and pressed into transparent sheets. Fourier Transform Infrared (FTIR) measurements in transmission mode were conducted using an FTIR spectrometer (Nicolet 5700, Thermo Scientific, USA). The wavelength range tested was 500–4000 cm^{-1}, with 32 scans for each sample.

2.2.2. Rheological testing

All samples were tested using a rotational rheometer (DHR 2, Waters, USA) with a plate diameter of 8 mm and a gap of 1 mm. Testing parameters used a fixed frequency of 1 Hz and a strain of 1 %. High and low cyclic strain testing alternated between 1 % (60 s) and 200 % (60 s) strain conditions, conducting three continuous cycles. The strain range was 1 %–1000 %, with a frequency of 1 Hz.

2.2.3. Scanning electron microscopy

The microstructure of G/H hydrogels was analyzed using a scanning electron microscope (SEM, Inspect F50, FEI, USA). The hydrogel was first treated with liquid nitrogen to fix its internal structure. Subsequently, the fixed hydrogel was freeze-dried, and the dried samples were placed on copper columns, sputtered with gold/palladium for 60 s, and then analyzed [14].

2.2.4. Injection ability, self-healing, and tissue adhesion testing

Macroscopic experiments were conducted to test injection ability, self-healing, and tissue adhesion. For the injection performance test, gelatin-ADH at a final concentration of 18 % and HA-CHO-SO_3 at a final concentration of 4 % were separately loaded into dual syringes and injected into continuous line marked as (I love FK), as well as circle and star-shaped molds with a radius of 10 mm and a thickness of 1 mm. Methylene blue and methyl orange were used for staining. For the self-healing test, different-colored hydrogel blocks were cut into certain shapes and swapped at specific time intervals (20 min), monitoring the hydrogel's self-healing behavior. Tissue adhesion tests were conducted using methyl orange to stain the hydrogel following two steps: 1) the O-shape hydrogels were tightly stacked to verify their fusion into an integrated tube; 2) the hydrogel tube was tightly adhered to freshly harvested rabbit tracheal segments to verify their adhesiveness to native trachea. All procedures were recorded using a camera.

The lap shear test was conducted on different hydrogel groups using a device with a 30 N load sensor. Fresh pig tissue was initially cut into rectangular shapes, each coated with 100 μL of the hydrogel solution. A second piece of tissue was then placed on top, forming an adhesive bond with an area measuring 25 mm by 10 mm. The test proceeded at a strain rate of 0.2 mm/s.

The various hydrogels were formed in cylindrical polytetrafluoroethylene molds with a diameter of 5 mm and a height of 3 mm. The compressive test was conducted at a displacement speed of 1 mm/s. The Young's Modulus was calculated using the linear segment of the stress-strain curve.

2.2.5. In vitro assessment of degradability

To evaluate the degradation behavior of the hydrogels, 100 μL of G/H, G/H-CD, G/sH, and G/sH-CD hydrogels were molded into cylinders with a diameter of 8 mm and then freeze-dried to obtain their dry weights (W_a). The hydrogel samples were then immersed in a trypsin solution with a concentration of 3 U/mL. After different time intervals, individual samples were removed from the solution, freeze-dried, and weighed for their dry weights (W_b). The degradation ratio was calculated using the following equation: $(W_b/W_a) \times 100$ %.

2.2.6. Cytokine release experiment

To study the release kinetics of KGN and TGFβ1 in different hydrogels, a basic control group of gelatin/HA hydrogel systems (G/H, G/sH, G/H-CD, G/sH-CD) was prepared. Gelatin-ADH was at a concentration of 18 %, HA-CHO or HA-CHO-SO_3 was at a final concentration of 4 %, and β-CD-CHO was at a final concentration of 0.5 %, with KGN and TGFβ1 concentrations as previously mentioned. Different hydrogels with a diameter of 10 mm and a height of 1 mm were soaked in 2 mL of PBS buffer. At specific time points (8 h, 12 h, 24 h, 3 days, 7 days, 14 days), 100 μL of the soaking solution was extracted and replaced with 100 μL of fresh PBS. The released KGN was measured at a wavelength of 280 nm using a spectrophotometer. The TGFβ1 content in the soaking solution was detected using a TGFβ1 enzyme-linked immunosorbent assay (ELISA) Kit (Elabscience, China), and release percentage curves for both active factors were plotted [15].

2.3. In vitro & In vivo experiments

2.3.1. Isolation and culture of BMSCs

BMSCs were harvested from 4-week-old male New Zealand white rabbits (Shanghai Yunde Experimental Farm). All animal experiments were conducted following the "Guidelines for the Care and Use of Laboratory Animals" and were approved by the Ethics Committee of Shanghai Pulmonary Hospital (K21-355Y). Under anesthesia, bone marrow was aspirated from the ilium using a heparinized syringe and transferred to centrifuge tubes. The bone marrow was diluted 1:1 with Dulbecco's Modified Eagle Medium (DMEM, Sigma, USA), centrifuged at 2000 rpm for 8 min, and the precipitate was collected. The collected bone marrow particles were cultured in DMEM containing 10 % fetal bovine serum (FBS, Sigma, USA) and 1 % antibiotics (Sigma, USA) at 37 °C in a 5 % CO_2 atmosphere. The medium was changed after 5 days to remove impurities and non-adherent cells, and the second-generation cells were harvested for subsequent use.

2.3.2. In vitro chondrogenic evaluation

The harvested BMSCs were incorporated into G/sH-CD, G/sH-CD + KGN, G + TGFβ1/sH-CD, G + TGFβ1/sH-CD + KGN hydrogels to achieve a final concentration of 5.0×10^5 cells/mL. The BMSC-laden hydrogels were then cultured in DMEM containing 10 % FBS and 1 % antibiotics at 37 °C in a 5 % CO_2 atmosphere for 14 days. Immunofluorescence staining was used to determine the distribution of collagen type II (COL II) and Recombinant Sex Determining Region Y Box Protein 9 (SOX9) in the four groups. Western blotting (WB) was employed to quantify the expression of different chondrogenic-related proteins COL II and SOX9. Briefly, samples were frozen in liquid nitrogen, tissue was pulverized using a high-speed disperser, cells were lysed and proteins were dissolved using RIPA buffer (Sigma-Aldrich, Germany). After separating and transferring to membranes, the proteins were incubated with appropriately diluted primary antibodies COL II (28459-1-AP, Proteintech, Wuhan, China) and SOX9 (67,439, Proteintech, Wuhan, China)), and the membranes were incubated with horseradish peroxidase-conjugated secondary antibodies. After washing thrice, an enhanced chemiluminescence solution (Thermo Fisher, USA) was used for visualization. The bands on the membranes were compared with molecular weight markers to determine protein presence [16]. Furthermore, real-time quantitative polymerase chain reaction (qRT-PCR) was conducted to assess the gene expression of *Col2a1* and *Sox9* using Glyceraldehyde-3-phosphate dehydrogenase (GAPDH) as the internal reference. Briefly, total RNA was extracted from the samples using TRIzol (Invitrogen, USA) and exposed to DNaseI (Fermentas, Canada) to remove any residual DNA. Subsequently, extracted RNA was reverse transcribed to cDNA using Prime Script Reverse Transcriptase (TakaRa, Japan), and qRT-PCR was performed using Ultra SYBR Mix (CWBIO, China). GAPDH was used as an endogenous control for $2^{\Delta\Delta CT}$ analysis. Primer sequences were synthesized using Oligo software and validated using BLAST software (Table S2, Supplemental information).

2.3.3. In vitro cell behaviors within hydrogels

The harvested BMSCs were suspended in DMEM containing 10 % FBS at a final concentration of 5×10^5 cells/mL. These BMSCs were then incorporated into G/sH-CD, G/sH-CD + KGN, G + TGFβ1/sH-CD, G + TGFβ1/sH-CD + KGN hydrogels and cultured in DMEM containing 10 % FBS and 1 % antibiotics at 37 °C in a 5 % CO_2 environment. To assess the viability and morphological characteristics of BMSCs in hydrogels, staining was performed using a live/dead staining kit (Invitrogen, USA), phalloidin (Yeasen, China), and 4,6-diamidino-2-phenylindole dihydrochloride (DAPI) on days 1 and 5 of cell culture [17]. Confocal microscopy (SP8X, Leica, Germany) was used to observe and capture images. The cell proliferation rate was determined using a Cell Counting Kit-8 (CCK-8, Abcam, USA) according to the manufacturer's instructions by measuring the absorbance at 450 nm using a spectrophotometer after incubation with CCK-8 reagent for 1 h on days 1 and 5. Additionally, DNA content was measured using a Quant-iT PicoGreen dsDNA Assay Kit (Life Technologies, USA) to further evaluate BMSC proliferation capability.

2.3.4. In vivo fused cartilage regeneration

Twelve healthy male 6-week-old New Zealand White rabbits, were divided into four groups: G/sH-CD, G/sH-CD + KGN, G + TGFβ1/sH-CD, G + TGFβ1/sH-CD + KGN. Hydrogel rings with O-shape were prepared by injecting BMSCs-laden hydrogels (in a concentration of 5.0×10^8 cells/mL) into annular molds with an inner diameter of 5 mm, a slot width of 1 mm, and a depth of 1 mm. Then, the prepared annular hydrogels were implanted subcutaneously in rabbits and retrieved after 4 weeks for chondrogenesis evaluation. Specifically, the obtained samples were fixed with 4 % polyformaldehyde for 24 h. After dehydration and paraffin embedding, cross sections of the regenerated cartilage rings were cut into 5 μm thick sections. Hematoxylin and eosin (H&E), Safranin-O, and immunohistochemical COL II staining were conducted to evaluate the cartilage deposition in various O-shaped hydrogels among G/sH-CD, G/sH-CD + KGN, G + TGFβ1/sH-CD, G + TGFβ1/sH-CD + KGN groups. In addition, GAG and COL II contents were determined using dimethylmethylene blue method and ELISA kit, respectively. Furthermore, the O-shaped samples were subjected to a compressive test to obtain their Young's modulus [18].

Subsequently, utilizing the self-healing ability of the hydrogel rings, a tubular hydrogel was prepared with the assistance of a silicone tube with an outer diameter of 5 mm. In addition, the tubular hydrogel was tightly adhered to fresh rabbit tracheal segment. Then, the prepared tubular configurations were implanted subcutaneously in rabbits and retrieved after 4 weeks for following evaluation. The H&E and Safranin-O staining were used to access the fused cartilage tissue using the individual hydrogel ring. In addition, the O-shaped sample from the G + TGFβ1/sH-CD + KGN group and a normal subcutaneous tissue (without any treatment) were subjected to immunofluorescence staining for CD68 and tumor necrosis factor-α (TNF-α) for *in vivo* inflammatory evaluation.

2.3.5. Sutureless anastomosis of LSTD reconstruction using hydrogel substitutes

Twenty male 6-week-old New Zealand White rabbits were randomly and equally divided into two groups, called sutured and unsutured groups. Four G + TGFβ1/sH-CD + KGN hydrogel rings with or without BMSCs (in a concentration of 5.0×10^8 cells/mL) load were assembled into a tubular configuration according to previously described method [19], in which the hydrogel rings were alternately placed on silicone tube with a diameter of 5 mm and a length of 2 cm to constitute hydrogel tubular configurations. The tubular configuration in sutured group was pre-embedded in the paracervical muscular space of the rabbit trachea for 4 weeks, and the obtained tubular substitute was used to reconstruct the LSTD via end-to-end anastomosis. The tubular configuration in unsutured group was used directly for LSTD reconstruction. Specifically, the rabbit trachea was exposed and 1 cm was intercepted to make a LSTD model, both ends of the hydrogel substitute were attached to the severed end of the trachea and securing the silicone tube in the lumen interior to the anastomosis with absorbable sutures. All experimental rabbits were given penicillin for 3 days after surgery to avoid infection. Two weeks after surgery, the experimented rabbits underwent surgery to remove the silicone stent. The survival rate of the experimented rabbits in sutured and unsutured groups were recorded over 6 weeks post-surgery. At 6 weeks, the experimental rabbits underwent tracheoscopy under anesthesia, and the patency rate and sputum blockage were assessed. In addition, the experimented rabbits were euthanized at 6 weeks post-surgery to obtain the reconstructed tracheal grafts for further analysis. All specimens along with native tracheas were photographed. H&E, safranin-O, and immunohistochemical COL II staining were used to evaluate cartilage-related characteristics. The expression levels of cytokeratin (CK, a specific marker for respiratory epithelial cells) were detected by immunofluorescence staining, and epithelial thickness was determined via the obtained immunofluorescence CK staining. COL II content was quantified using enzyme-linked immunosorbent assay, and Young's modulus was analyzed using a compressive test.

2.4. Statistical analysis

All quantitative data are presented as the means ± standard deviations. Data were obtained from as least 3 parallel experiments and analyzed using GraphPad Prism 5.0 by one-way ANOVA, and $p < 0.05$ was considered statistically significant.

3. Results and discussion

3.1. Preparation and characterization of G/H hydrogel

The preparation and characterization of the G/H hydrogel involved the utilization of natural macromolecules, namely HA and gelatin. The chemical structure of modified HA and gelatin and the crosslinking formation of the G/H hydrogel was illustrated in Fig. S1. The HA underwent oxidation via $NaIO_4$, transforming it into aldehyde-modified HA (HA-CHO), followed by sulfonation with SO_3-pyridine, resulting in HA-CHO-SO_3. As shown in Fig. S2, the resulting aldehyde group content was 0.859 mmol/g for HA-CHO and 0.864 mmol/g for HA-CHO-SO_3, indicating the sulfation did not negatively affect the aldehyde modification of HA. The FTIR analysis depicted specific peaks: CHO at 1727 cm^{-1}, a distinctive S=O band at 1190 cm^{-1}, and a C-O-S peak at 880 cm^{-1}, affirming successful aldolization and sulfonation of HA (Fig. S3). Elemental analysis further indicated a sulfonation content of 0.66 mmol/g for HA-CHO-SO_3 (Table S3, Supplemental Information). Concurrently, gelatin's carboxyl group was activated through EDC/HOBT to create amidated gelatin (gelatin-ADH). FTIR analysis of the resultant product displayed peaks corresponding to N-N stretching vibrations at 3155 cm^{-1} and 3025 cm^{-1}, validating successful ADH grafting onto gelatin (Fig. S4).

These modified components, namely HA-CHO and Gelatin-ADH, contained active groups capable of forming dynamic Schiff base covalent bonds via reversible condensation reactions under specific conditions. This dynamic equilibrium in covalent bonding formed the foundation for the exceptional mechanical properties and self-healing function achieved by combining these hydrogels. To enhance the drug loading rate of KGN, aldolylated β-cyclodextrin (β-CD-CHO) was introduced into the system. β-CD, a cyclic oligosaccharide, possesses a hydrophobic cavity suitable for binding with KGN, facilitating a host-guest interaction to enhance KGN stability. $NaIO_4$ conversion of β-CD into β-CD-CHO initiated a condensation reaction with gelatin-ADH, further enhancing the drug loading rate and bioavailability of KGN. The FTIR confirmation illustrated the successful aldolization of β-CD, as evidenced by the presence of the -CHO absorption peak at 1726 cm^{-1} (Fig. S5).

3.2. Rheological analysis of G/H hydrogel

To identify the most suitable hydrogel substrate for tracheal reconstruction, excluding β-CD-CHO and -SO_3, we conducted rheological tests by mixing different concentrations of gelatin-ADH and HA-CHO in a 1:1 ratio. Based on previous knowledge, the gelatin-ADH concentration ranged from 8 % to 18 %, while the HA-CHO concentration was set at either 2 % or 4 %. Across various hydrogel compositions, the elastic modulus (G′) consistently surpassed the viscous modulus (G″), affirming successful gelatinization of all Gelatin-ADH and HA-CHO-based hydrogels (Fig. 1a and b). Moreover, elevating the gelatin-ADH concentration corresponded to increased G′ and G″ values, which might be contributed to the intensified crosslinking of Schiff base bonds and the increased solid composition concentration. Notably, among all combinations, G_{16}/H_4 and G_{18}/H_4 exhibited superior elastic moduli, with G_{18}/H_4 displaying a better viscous modulus. To assess the self-healing ability of the G_{18}/H_4 hydrogel, we subjected it to varying shear strains from 1 % to 200 % for defined durations. Remarkably, the G′ and G″ of the G_{18}/H_4 hydrogel consistently reverted to their initial levels, underscoring its excellent self-healing properties (Fig. 1c). Rheological strain scans revealed that the G′ and G″ of the G_{18}/H_4 hydrogel did not intersect until reaching 100 % stress conditions. This observation signifies that the internal network of this hydrogel remains stable at strains below 100 %, meeting the criteria for tracheal repair and reconstruction (Fig. 1d). Consequently, G_{18}/H_4 was selected as the hydrogel backbone for subsequent experiments.

3.3. Injectability, self-healing and adhesive properties of G/H hydrogel

The injectability of the G/H hydrogel was achieved by effectively extruding it through a syringe to inscribe the abbreviation "I love FK" (Fig. 2a). This method was particularly useful in preparing O-shaped hydrogel rings, meeting our specific needs.

The imine linkage, known as the Schiff base bond, results from the reversible condensation reaction between a primary amine (R-NH_2) and a reactive carbonyl group (e.g., aldehyde, ketone). This bond breaks under external forces but swiftly regenerates. Leveraging the reversible condensation reaction between the abundant free amino and aldehyde groups on the side chains of aldehyde-modified HA and hydrazide-modified gelatin molecules, we achieved the gelation and self-healing properties of the hydrogels (Fig. S6). To confirm this, we initially prepared two-component hydrogels of varying shapes using specific G_{18}/H_4 concentration ratios. Subsequently, we exchanged and cut the pre-shaped hydrogels. After 20 min, the recombined hydrogels seamlessly healed, merging to form a new unit. The pigments between the interfaces blended without distinct demarcation lines (Fig. 2b).

Additionally, the surface of proteins in natural tissues, rich in free amino groups, can react with aldehyde-modified HA inside the hydrogel, leading to strong adhesion. Upon contact between the hydrogel trachea substitutes and fresh rabbit tracheal tissues, we observed firm adhesion of the substitutes to the tracheal stumps (Fig. 2c). These substitutes remained secure and resistant to displacement even under external force application (Video S1). Subsequent SEM examination of the interconnected hydrogel interfaces revealed a solid, tight healing interface between adjacent hydrogels (Fig. 2d).

The lap-shear method was used to test the tissue adhesive strength of G/H, G/H-CD, G/sH, and G/sH-CD hydrogels. The results showed that the tissue adhesive strength of these hydrogels was approximately 28 kPa, with the G/sH-CD hydrogels demonstrating the highest tissue adhesive strength (Fig. S7). In addition, the Young's modulus of these hydrogels was about 7 kPa (Fig. S8) in a compressive test. This property streamlines future tracheal replacement procedures by reducing the need for surgical sutures, significantly simplifying the surgical process, and greatly facilitating the widespread implementation of tracheal surgery.

3.4. In vitro cytokines release kinetic of G + TGFβ1/sH-CD + KGN hydrogel

The biodegradability of hydrogel is crucial for the sustained release of its encapsulated cytokines. The *in vitro* degradation rate curves of G/H, G/H-CD, G/sH, and G/sH-CD hydrogels, shown in Fig. S9, indicate

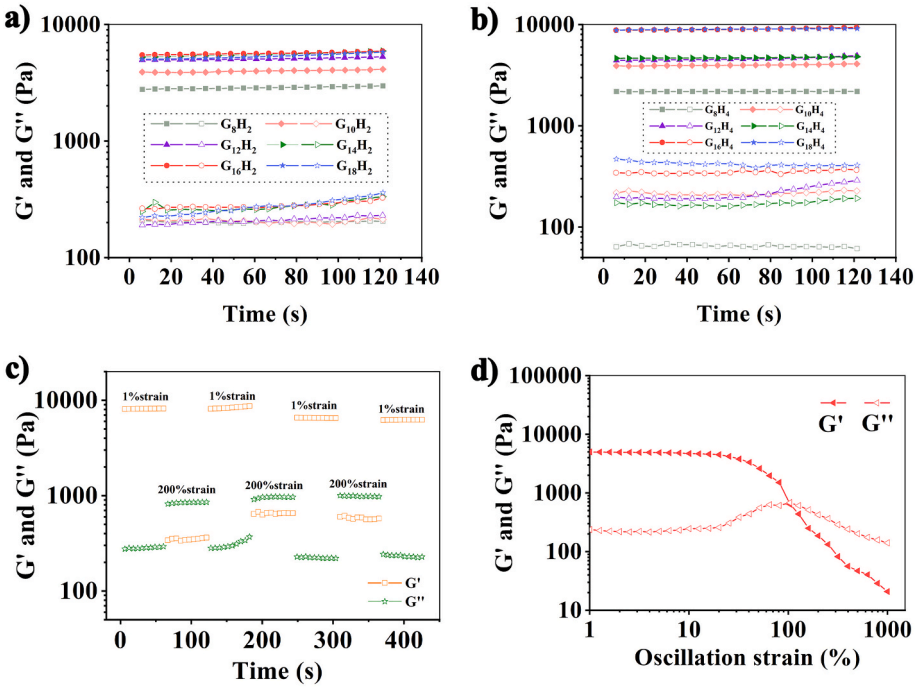

Fig. 1. Rheological analysis of the G/H hydrogels. Rheological time sweep test of (a) GxH_2 and (b) GxH_4 hydrogels, in which x marks 8, 10, 12, 14, 16, and 18. The solid symbols represented G′ and the hollow symbols represented G''. (c) Rheological cyclic low-high strain of G_{18}/H_4 hydrogel. (d) Rheological strain sweep test of G_{18}/H_4 hydrogel at 37 °C atmospheres.

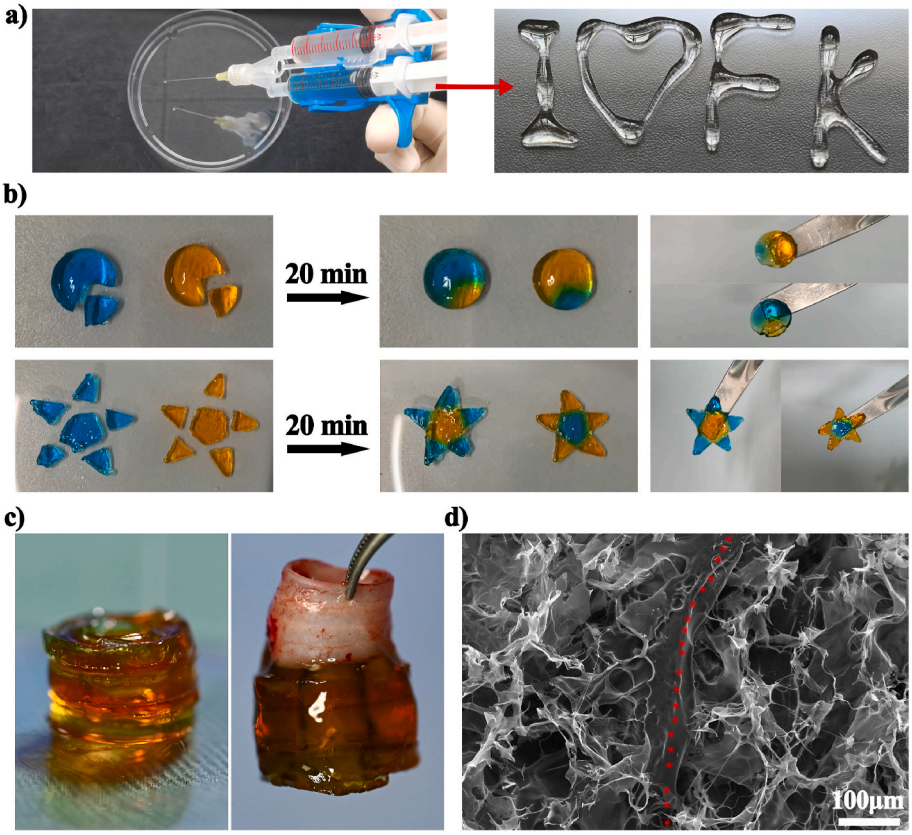

Fig. 2. Injectability, self-healing and adhesive properties of the G/H hydrogels. (a) The injectable behavior demo of G/H hydrogel. (b) The self-healing process of G/H hydrogel in different models. (c) The adhesive tests of G/H hydrogel to G/H hydrogel (left panel) and G/H hydrogel to rabbit tracheal tissue (right panel). (d) SEM image of the freeze-dried connection part of self-healed G/H hydrogel, in which the dotted red line marks the adjacent between the G/H hydrogels.

significant degradation when incubated in a trypsin solution. Notably, these hydrogels were almost completely degraded after 700 h of incubation, with no significant differences observed among the four hydrogel groups. To establish an optimal microenvironment for BMSCs differentiation and proliferation within the hydrogel, we incorporated two cytokines, KGN and TGFβ1, synergistically fostering stable chondrogenesis. To extend the cytokine release period, covering BMSCs' proliferation, differentiation, and cartilage maturation, we employed sulfonation and β-CD encapsulation techniques to enable a slow release of these chondrocytokines. We evaluated four hydrogel formulations (G/H, G/sH, G/H-CD, and G/sH-CD) for their *in vitro* release profiles of KGN and TGFβ1 over 2 weeks. The results indicated that none of the four hydrogels released over 30 % of TGFβ1 within 2 weeks. Notably, -SO_3 presence (G/sH and G/sH-CD) significantly mitigated the initial burst release of TGFβ1 within the first 24 h compared to hydrogels lacking -SO_3 (G/H and G/H-CD) (Fig. 3a). This reduction in burst release is attributed to the strong negative charge of the -SO_3 group in the HA hydrogel backbone, enabling electrostatic interactions with TGFβ1, facilitating its firm adsorption and impeding burst release.

Concurrently, the release test revealed complete KGN release within 1 week from hydrogels without β-CD-CHO (G/H and G/sH), whereas hydrogels with β-CD-CHO (G/H-CD and G/sH-CD) retained approximately 20 % of the drug loading capacity at 2 weeks (Fig. 3b). This suggests that incorporating β-CD-CHO significantly extended the KGN release cycle. β-CD-CHO, binding to the main bond of gelatin, possesses an internal hydrophobic region facilitating a host-guest interaction with KGN, thereby slowing down its release rate from the hydrogel interior. These outcomes underscore the substantial enhancement in sustained release rates of KGN and TGFβ1 with the introduction of -SO3 and β-CD-CHO. The prolonged release of these chondrocytokines allows ample time for BMSCs differentiation into chondrocytes and the maturation of regenerated cartilage.

3.5. *Chondrogenic effect of G + TGFβ1/sH-CD + KGN hydrogel*

TGFβ1 plays a vital role in steering stem cell differentiation toward chondrocytes, serving as a crucial component in the *in vitro* chondrogenic process. However, it possesses a dual nature, inducing stem cell hypertrophy, detrimental to stable cartilage maintenance [20]. To address this, we introduced KGN, a stable hydrophobic small molecule known for promoting cartilage repair and inhibiting stem cell-induced chondrocyte hypertrophy, both *in vitro* and *in vivo* [21]. Through the combined action of these two chondrocytokines, stable cartilage formation is jointly promoted.

Through the investigation of the synergistic mechanism of KGN and TGFβ1, it has been found that KGN treatment specifically increases the phosphorylation of Smad2/3, differing from the effect of TGFβ1, but does not significantly affect the phosphorylation of Smad1/5/8 [22]. KGN promotes the chondrogenic differentiation of BMSCs by interacting with the actin-binding protein filamin A (FLNA). KGN binds to the FC-1 fragment of FLNA, releasing core binding factor beta subunit (CBFβ) from its cytoplasmic binding site. Consequently, CBFβ enters the nucleus, where it binds to Runx factors, regulating the transcription of chondrogenesis-related proteins and genes through the CBFβ-Runx1 transcriptional program [23]. Meanwhile, it is known that Runx2 directs osteoblast differentiation and chondrocyte hypertrophy, thereby reducing the regeneration effect of tracheal cartilage. The CBFβ-Runx1 transcriptional program may also help maintain relatively low levels of Runx2, thus sustaining chondrogenesis function. These studies suggest that KGN may promote the chondrogenesis of BMSCs through Runx1-mediated transcriptional effects, partially by activating the TGFβ1-Smad2/3 pathway and inhibiting Runx2 expression [24,25].

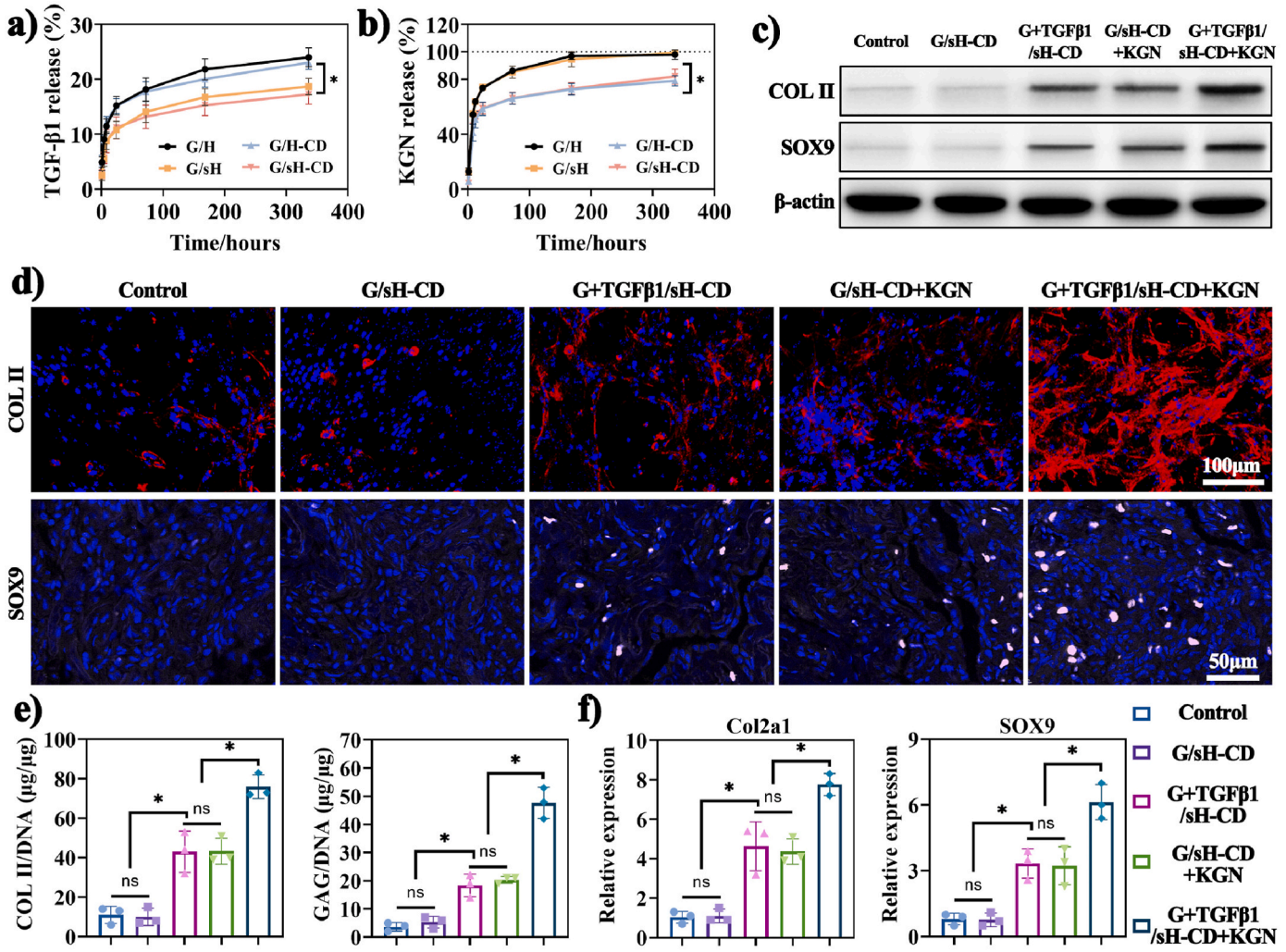

Fig. 3. ***In vitro*** **release curves and chondrogenic capacity of G + TGFβ1/sH-CD + KGN hydrogel.** *In vitro* cumulative release curves of TGFβ1 (a) and KGN (b) in G/H, G/H-CD, G/sH, and G/sH-CD hydrogels after incubated in PBS (pH = 7.4) over 8 h to 14 days. (c) The expression levels of chondrogenic-related proteins (COL II and SOX9) in different groups via WB examination. (d) Immunofluorescence staining of COL II and SOX9 proteins for BMSCs-loaded hydrogels after 14 days *in vitro* culture. (e) COL II and GAG normalized to DNA in BMSCs-loaded hydrogels after 14 days *in vitro* culture. (f) Relative expression of chondrogenic-related genes (*Col2a1* and *Sox9*) in BMSCs-loaded hydrogels after 14 days *in vitro* culture via qRT-PCR examination. *, $p < 0.05$; ns, no statistical significance.

Considering the TGFβ1 signaling pathway, it is reasonable that the combined use of KGN and TGFβ1 can achieve the effect of inducing chondrogenic differentiation and inhibiting hypertrophy in BMSCs.

To assess the chondrogenic capacity of the G + TGFβ1/sH-CD + KGN hydrogel, BMSCs were loaded into four distinct hydrogels (G/sH-CD, G + TGFβ1/sH-CD, Gs/H-CD + KGN, and G + TGFβ1/sH-CD + KGN) and cultured *in vitro* for 14 days. Results from WB examinations revealed elevated expression levels of COL II and SOX9 proteins in chondrocytes within the G + TGFβ1/sH-CD + KGN group compared to the control and other groups (Fig. 3c). Immunofluorescence staining further demonstrated increased secretion of COL II and SOX9 in the G + TGFβ1/sH-CD + KGN group compared to the other groups (Fig. 3d).

To mitigate discrepancies in hydrogel volume and cell density, we normalized the total DNA amount and observed significantly higher rates of COL II/DNA and GAG/DNA synthesis in the dual cytokine-loaded hydrogel group, underscoring the synergistic promotional effect of these cytokines (Fig. 3e). qRT-PCR assays confirmed these findings, with the G + TGFβ1/sH-CD + KGN group exhibiting the highest expression levels of chondrogenic genes (*Col2a1* and *Sox9*) (Fig. 3f). SOX9 protein serves as a crucial marker during chondrocyte differentiation [26], while COL II constitutes the primary collagen component in hyaline cartilage [27]. These outcomes affirm that dual cytokine-loaded hydrogels effectively induce BMSCs differentiation into chondrocytes, contributing to hyaline cartilage secretion, laying a robust foundation for in situ tracheal cartilage regeneration.

3.6. *In vitro cell behaviors of G + TGFβ1/sH-CD + KGN hydrogel to BMSCs*

The biocompatibility of the G + TGFβ1/sH-CD + KGN hydrogel is crucial for its application in tissue engineering [28,29]. To assess this, BMSCs were *in vitro* cultured on the G + TGFβ1/sH-CD + KGN hydrogel for 5 days, and various assays were conducted including live/dead assays, F-actin staining, and CCK-8 assays.

Live/dead cell staining revealed that the inclusion of KGN and TGFβ1 cytokines didn't notably affect BMSCs' proliferation, showing no significant cell death across the four hydrogel types (Fig. 4a) over 1–5 days. F-actin staining demonstrated that BMSCs within all hydrogel groups exhibited favorable stretched morphological characteristics, similar to the control group (Fig. 4b).

Quantitative assessments via CCK-8 assays and DNA content quantification indicated robust proliferation of BMSCs within all hydrogels, affirming excellent cell compatibility (Fig. 4c and d). These outcomes collectively indicate that G + TGFβ1/sH-CD + KGN hydrogels, as three-

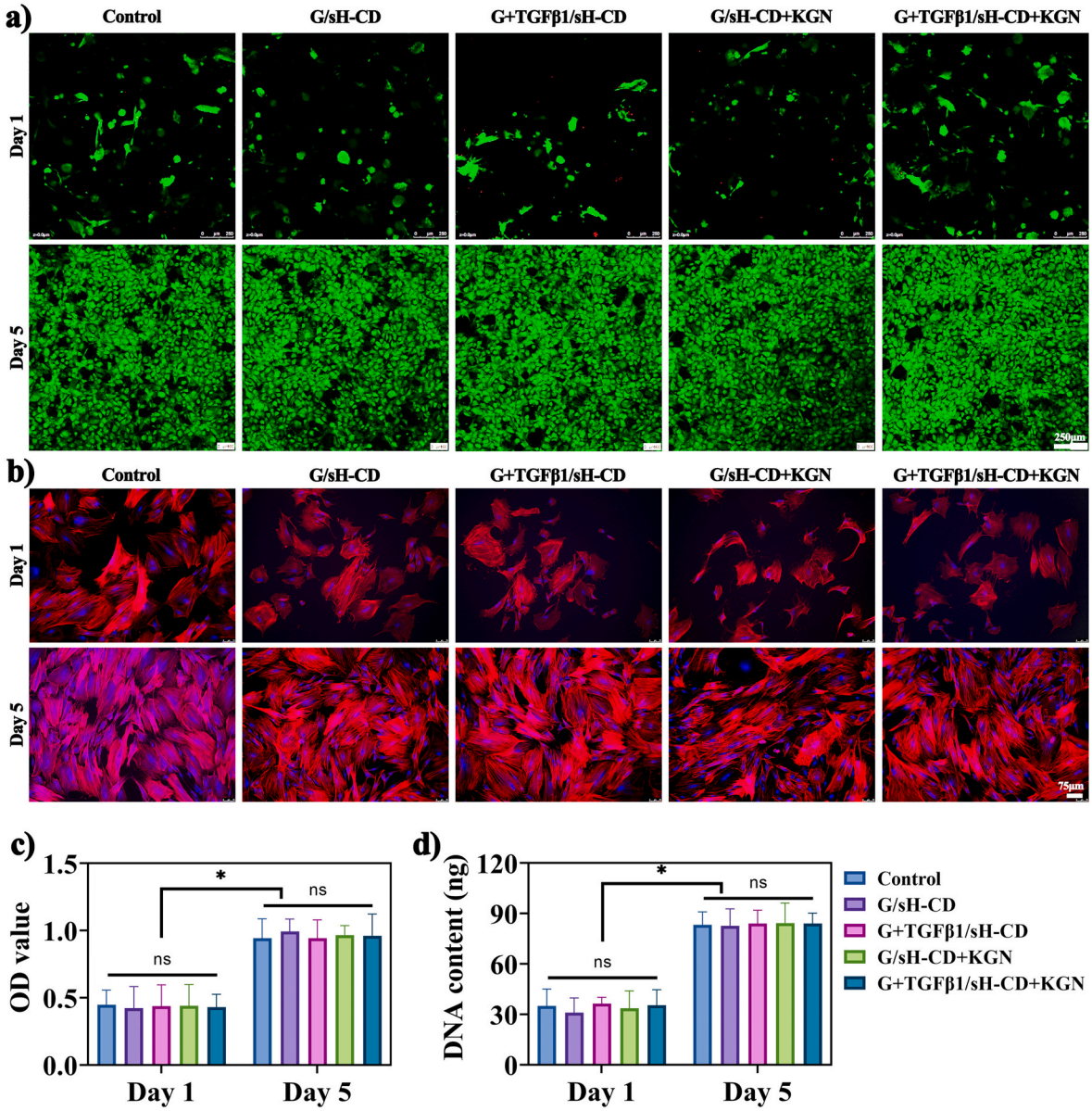

Fig. 4. ***In vitro*** **biocompatibility evaluation of G + TGFβ1/sH-CD + KGN hydrogel to BMSCs on day 1 and day 5.** (a) Live/dead staining of BMSCs in control, G/sH-CD, G + TGFβ1/sH-CD, G/sH-CD + KGN, G + TGFβ1/sH-CD + KGN hydrogels. (b) F-actin/DAPI staining of BMSCs in control, G/sH-CD, G + TGFβ1/sH-CD, G/sH-CD + KGN, G + TGFβ1/sH-CD + KGN hydrogels. (c) Quantification analysis of OD value via the CCK-8 assay in various BMSCs-loaded hydrogels. (d) Quantitative analysis of DNA content in various BMSCs-loaded hydrogels. *, $p < 0.05$; ns, no statistical significance.

dimensional cell culture scaffolds, possess commendable biocompatibility. The porous three-dimensional structure facilitates BMSCs' accommodation, survival, and proliferation, creating an optimal environment for subsequent deposition of the cartilage matrix.

3.7. *In vivo fused cartilage regeneration*

To assess the *in vivo* chondrogenic potential of drug-loaded hydrogels in inducing BMSCs, we implanted O-shaped BMSC-loaded hydrogels into the subcutaneous skin of rabbits. After 4 weeks, regenerated cartilage rings were retrieved for evaluation (Fig. S10a). Gross observations revealed the formation of white cartilaginous structures in all four types of BMSC-loaded hydrogel rings (Fig. 5a). However, histological analyses (H&E, Safranin-O, and immunohistochemical COL II staining) indicated varying degrees of cartilage-specific extracellular matrix formation (Fig. 5b and Figs. S11a–c). The G/sH-CD hydrogel without cytokine induction showed loose cartilage matrix, suggesting partial differentiation of BMSCs into chondrocytes. Incorporating single KGN or TGFβ1 in G + TGFβ1/sH-CD and G/sH-CD + KGN hydrogels improved chondrocyte characteristics and neocartilage deposition compared to the G/sH-CD hydrogel. Remarkably, the G + TGFβ1/sH-CD + KGN hydrogel, with dual KGN and TGFβ1 encapsulation, demonstrated optimal cartilage regeneration. This was evidenced by extensive cartilage-specific lacuna and high COL II content.

Quantitative analysis confirmed that regenerated cartilage rings in G + TGFβ1/sH-CD + KGN hydrogel displayed COL II and GAG levels comparable to natural tracheal cartilage, significantly higher than single cytokine or cytokine-free hydrogels (Fig. 5c and d). Moreover, Young's modulus results showed superior mechanical properties in the regenerated cartilage ring of the G + TGFβ1/sH-CD + KGN group compared to other hydrogel groups, with no significant differences compared to native tracheal cartilage rings (Fig. 5e). This superior mechanical property suggests its suitability as a tracheal repair substitute.

To explore fused cartilage tissue generation, multiple BMSC-loaded

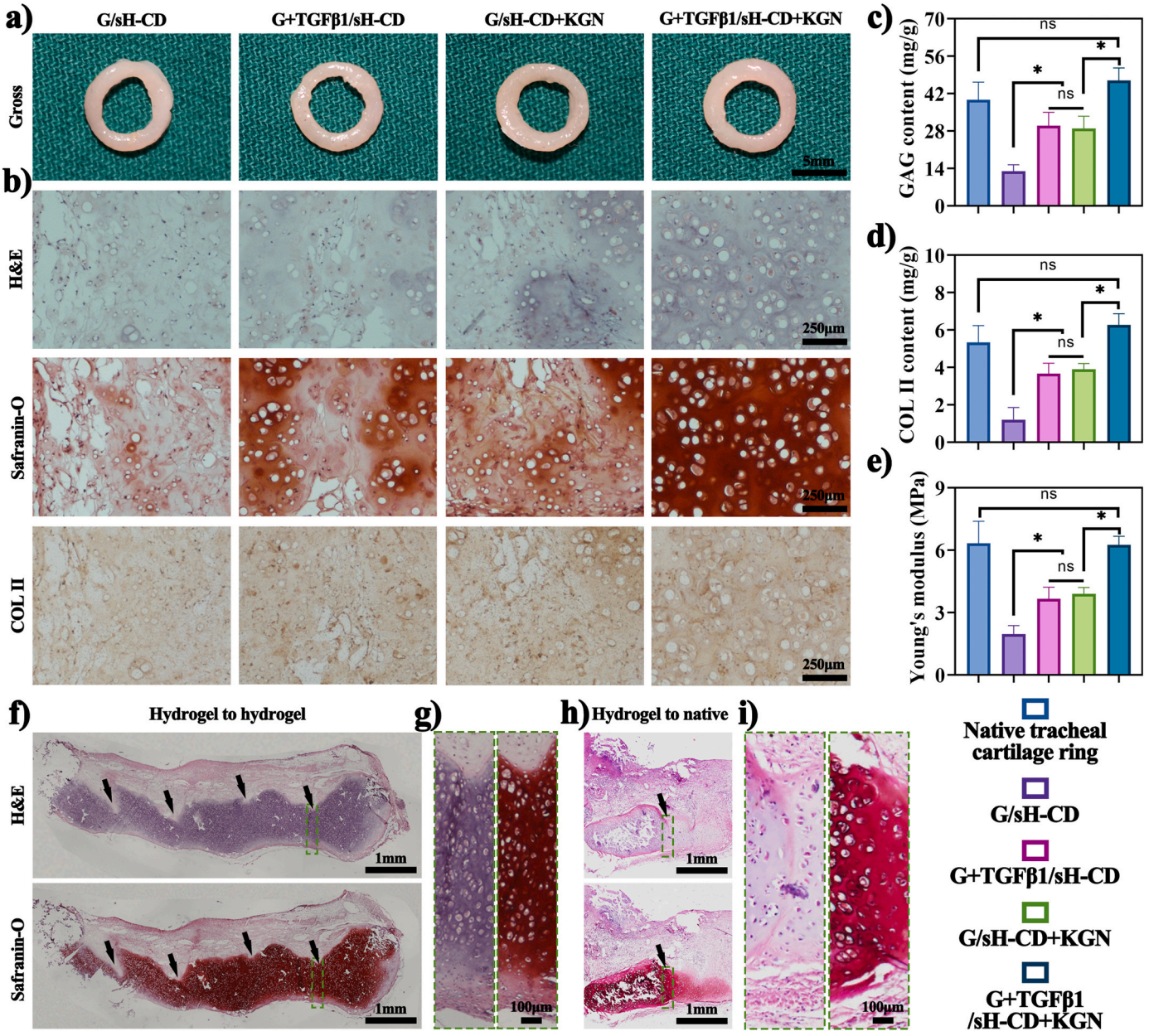

Fig. 5. ***In vivo*** **evaluations of chondrogenesis and fused cartilage regeneration using BMSC-laden G + TGFβ1/sH-CD + KGN hydrogel in a rabbit.** (a) Gross view, (b) H&E, Safranin-O, and immunohistochemical COL II stainings of BMSCs-loaded hydrogels with O-shape in various groups after 14 days of subcutaneous implantation. Quantification of (c) GAG content, (d) COL II content, and (e) Young's modulus for BMSCs-loaded hydrogels with O-shape in native tracheal cartilage ring and various hydrogel groups after 14 days subcutaneous implantation (*, $p < 0.05$; ns, no statistical significance). (f–g) Evaluation of the ability to regenerate fused cartilage using several self-healed O-shaped BMSCs-loaded G + TGFβ1/sH-CD + KGN hydrogels after 28 days of subcutaneous implantation, in which images in g are the magnified images of green dotted squares outlines zone in f. Black arrows marks the border between O-shaped BMSCs-loaded hydrogels. (h–i) Evaluation of the ability to regenerate fused cartilage using O-shaped BMSCs-loaded G + TGFβ1/sH-CD + KGN hydrogel adhered to native tracheal ring after 28 days of subcutaneous implantation, in which images in i are the magnified images of green dotted squares outlines zone in h. Black arrows marks the border between BMSCs-loaded hydrogel and native tracheal ring.

hydrogels with O-shape were stacked and implanted into rabbits for 4 weeks (Fig. S10b). Results demonstrated that newborn cartilage in adjacent hydrogel regions fused, forming a continuous cartilage structure (Fig. 5f and g). This suggests the self-healing ability of the G + TGFβ1/sH-CD + KGN hydrogel not only achieved surface integration but also internally fused newborn cartilage scaffolds.

Simultaneously, circular hydrogels adhered to freely available tracheal cartilage rings were subcutaneously embedded (Fig. S10c). Regenerated cartilage observed after 4 weeks exhibited integration with adjacent natural cartilage areas (Fig. 5h and i). This indicates that G + TGFβ1/sH-CD + KGN hydrogels not only possess excellent tissue adhesion but also exhibit compatibility after adhesion with natural tissue, enabling seamless healing between regenerated and natural tracheal cartilage. This demonstrates the potential use of BMSC-loaded hydrogels to facilitate tracheal anastomoses *in vivo* without suturing.

To more directly observe the biocompatibility of the G + TGFβ1/sH-CD + KGN hydrogel *in vivo*, samples from the subcutaneously implanted G + TGFβ1/sH-CD + KGN hydrogel and BMSCs in rabbits were subjected to immunofluorescence staining for CD68 (a macrophage marker) and TNF-α (an inflammatory marker). Our data indicated that the positively stained CD68 and TNF-α markers were comparable between the normal tissue and G + TGFβ1/sH-CD + KGN hydrogel groups (Fig. S12), further

demonstrating the favorable biocompatibility of the G + TGFβ1/sH-CD + KGN hydrogel *in vivo*.

3.8. Sutureless anastomosis for LSTD reconstruction with hydrogel substitute

The preceding studies involved the placement of engineered tracheal cartilage substitutes in the paracervical area and subsequent anastomosis to the natural airways using interrupted sutures once the substitutes stabilized [19,30]. However, while this approach achieved short-term patency, long-term success was limited due to extensive granulomatous tissue proliferation around the anastomosis postoperatively [31]. To overcome this, we devised a novel tracheal defect repair method leveraging the self-healing capability of hydrogels to adhere to autologous tissues. This method negates the need for surgical suturing at the anastomosis site.

In this study, we arranged both BMSCs loaded and unloaded hydrogels in an O-shape using our previously established ring-to-tube method to create a tracheal substitute. Following 4 weeks of submuscular implantation, the synthesized tracheal substitutes were utilized for LSTD reconstruction. We employed two approaches: one involving traditional end-to-end anastomosis (termed as the sutured group) [32], and the other method directly attaching the synthesized tracheal substitute to the LSTD using a sutureless anastomosis (termed as the unsutured group) (Fig. 6a and Fig. S13). Fig. 6b illustrates the technique of sutureless anastomosis for LSTD reconstruction using a hydrogel tracheal substitute.

Subsequent tracheoscopy performed at the 6-week mark highlighted notable differences between the two groups. The end-to-end anastomotic reconstruction group showed severe anastomotic stenosis, while the unsutured surgery group exhibited only mild elevation at the anastomotic interface, whereas the sutured group presented an obvious narrow anastomosis (Fig. 6c). Further examination revealed distinct variations in tissue response. The sutured group displayed severe

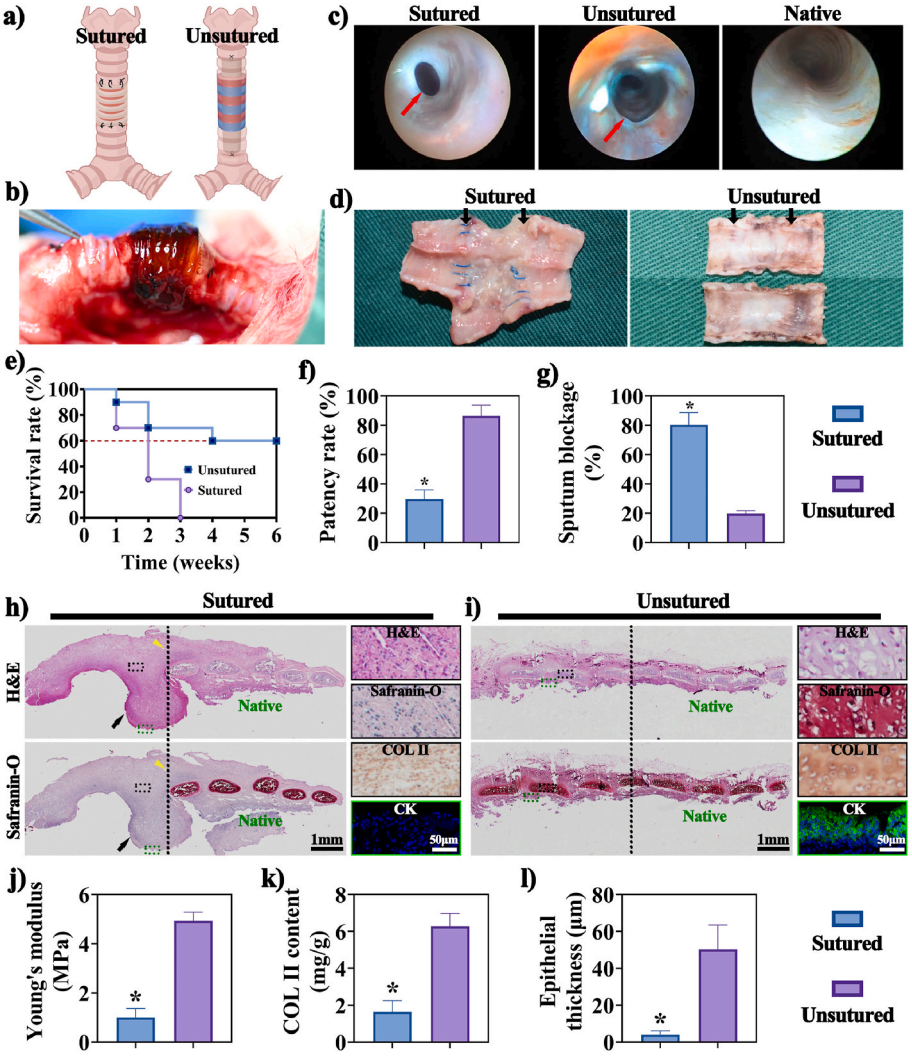

Fig. 6. Sutureless LSTD reconstruction using BMSCs-loaded G + TGFβ1/sH-CD + KGN hydrogel tracheal substitute in a rabbit. (a) Schematic illustration for LSTD reconstruction via sutured and unsutured procedures. (b) Photograph for BMSCs-loaded G + TGFβ1/sH-CD + KGN hydrogel tube for LSTD reconstruction with unsutured procedure. (c) Bronchoscope examination of tracheal lumen in sutured, unsutured, and native trachea groups, in which the red arrows denote the anastomosis. (d) Photograph for transplanted trachea in sutured and unsutured groups after 6 weeks LSTD reconstruction. Black arrows denote the anastomosis. (e) Survival rate of experimental rabbits in the sutured and unsutured groups 6 weeks after LSTD reconstruction. (f–g) Quantification of patency rate and sputum blockage in the sutured and unsutured groups (*, $p < 0.05$). (h–i) Overview of the transplanted trachea in sutured and unsutured groups with H&E and Safranin-O staining, shown in the left panels. Magnified views of the regions marked by black-dotted squares are shown with H&E, Safranin-O, and immunohistochemical COL II staining, as illustrated in the right panels. Similarly, magnified views of the green-dotted squares show immunofluorescence CK staining, also depicted in the right panels. Black dotted lines indicate the anastomosis, and black arrows point to granulation tissue hyperplasia. (j–l) Quantification of Young's modulus, COL II content, and epithelial thickness in sutured and unsutured groups (*, $p < 0.05$).

granulomatous hyperplasia and sputum-covered surfaces, whereas the unsutured group presented a smooth, regenerating tracheal lumen devoid of granulated tissue (Fig. 6d). Notably, the unsutured group exhibited significantly higher postoperative survival and patency rates compared to the sutured surgery group at the 6-week mark (Fig. 6e and f). Quantitative analysis further supported these findings, indicating a lower percentage of sputum blockage in the unsutured group compared to the sutured group (Fig. 6g).

Histological analysis of excised tracheas unveiled distinct differences between the unsutured and sutured groups. The sutured group displayed persistent mucus accumulation due to the poor mechanical compliance of the new trachea, leading to prolonged inflammation, gradual replacement of chondrocytes by fibroblasts, granulation tissue hyperplasia, and an unfavorable environment for endothelial cell migration (Fig. 6h). Conversely, the unsutured group showcased well-defined cartilaginous structure, evident cartilage lacunae in H&E and Safranin-O staining, abundant COL II content, and newly formed tracheal epithelium on the hydrogel's inner surface (Fig. 6i).

Quantitative analysis of Young's modulus, COL II content, and epithelium thickness at the observation endpoint favored the unsutured group (Fig. 6j–l), demonstrating higher elasticity, richer COL II content, and accelerated re-epithelialization compared to the sutured surgery group. This suggests that the unsutured anastomosis significant inhibit granulation tissue hyperplasia, better maintains the new cartilage, and fosters a smooth lumen conducive to endothelial cell migration, providing a stable foundation for functionalized LTSD reconstruction.

The tracheal diameter dynamically changes during breathing, influenced by the diaphragm's movement during expiration and inspiration, responding to pressure changes within the thoracic cavity [33]. Earlier attempts at creating newborn cartilage rings, despite their elasticity and biomimetic qualities, failed to seamlessly match the autogenous trachea, causing pressure differences near the anastomosis. This led to friction between tissues during respiratory movements, ultimately causing inflammation and fibrosis [34,35].

While the use of β-CD-conjugated hydrogel for drug delivery has been reported, there are still few reports on dual drug delivery systems based on this hydrogel. Moreover, there are no articles on the use of β-CD-conjugated hydrogel for tracheal repair. For effective tracheal repair, it is crucial to achieve the alternating formation of cartilage and fibrous tissue. In our work, we are the first to utilize the exceptional self-healing properties of hydrogel to promote tracheal regeneration with a unique structure of alternating cartilage and fibrous tissue. This is accomplished by alternately stacking BMSCs-loaded hydrogel rings with cell-free hydrogel rings.

Furthermore, studies indicate the sensitivity of airway epithelium to mechanical forces and the benefits of appropriate stretching and compression exercises in maintaining airway health [36,37]. However, fully chondrogenic tracheal substitutes, due to their rigidity, hinder normal tracheal epithelium stretching, impeding its proliferation. The airway epithelium, vital as a natural barrier, aids in particle clearance and smooth sputum expulsion. Hence, a compliant tracheal substitute not only reduces granulation tissue proliferation resulting from mismatched anastomotic mechanics but also fosters endothelial proliferation, crucial for infection prevention and reducing sputum buildup.

Surgical sutures, acting as foreign bodies, trigger the recruitment of macrophages and neutrophils around the anastomosis, sparking acute inflammatory responses leading to anastomotic stenosis or dehiscence [38,39]. Despite attempts to improve anastomotic healing—tension-reducing sutures, tissue wraps, and sealants—clinical complications still arise in about 10 % of patients [40]. Hence, we opted for an adhesive technique in tracheal defect reconstruction. This eliminates suture-related issues, avoiding acute inflammatory reactions due to foreign body irritation. The sutureless approach results in a smoother anastomotic lumen, further aiding endothelial cell migration and sputum expulsion.

4. Conclusion

This study introduces a self-healing hydrogel with potent chondrogenic properties designed to tackle early anastomotic stenosis and facilitate sustained, healthy tracheal cartilage regeneration. The G + TGFβ1/sH-CD + KGN hydrogel demonstrates robust self-healing capabilities, attributed to its strong covalent bonding network of acylhydrazones between hydrazide and aldehyde groups. This network significantly contributes to the hydrogel's exceptional self-repairing abilities. In experiments involving a rabbit model with LSTD, the hydrogel's Schiff base reaction with the tissue's amino group facilitated sutureless anastomosis of the tracheal substitute. Additionally, the sustained release of dual chondrogenic agents in the presence of BMSCs led to remarkable tracheal cartilage regeneration. The BMSC-loaded G + TGFβ1/sH-CD + KGN hydrogels were molded into a malleable tracheal substitute using our established ring-to-tube method. This innovative approach enabled the repair of LSTD without sutures, resulting in reduced early postoperative anastomotic stenosis, maintained long-term tracheal patency, decreased instances of sputum blockage, promoted reepithelization, and ensured stable tracheal cartilage regeneration. Remarkably, it also increased the survival rate of the experimental rabbits. Therefore, the utilization of self-healing hydrogels with chondrogenic capacity signifies a significant leap forward in sutureless tracheal anastomosis and tracheal cartilage regeneration. This approach holds promising potential for inhibiting early postoperative anastomotic stenosis and tracheal chondromalacia in the treatment of LSTD.

CRediT authorship contribution statement

Liang Guo: Writing – original draft, Visualization, Validation, Data curation. **Xuezhe Liu:** Writing – review & editing, Writing – original draft, Visualization, Validation, Methodology, Data curation. **Yao Wang:** Writing – review & editing, Writing – original draft, Visualization, Validation, Project administration, Methodology, Data curation. **Jiaoyu Yi:** Software. **Juanjuan Li:** Formal analysis. **Yong Xu:** Formal analysis, Data curation. **Kaiyong Cai:** Investigation. **Wufei Dai:** Writing – review & editing, Resources. **Qian Feng:** Writing – review & editing, Writing – original draft, Supervision, Funding acquisition. **Bo Tao:** Writing – review & editing, Supervision, Methodology, Investigation, Funding acquisition.

Declaration of competing interest

The authors declare no conflict of interest.

Data availability

No data was used for the research described in the article.

Acknowledgements

This research was supported by the National Natural Science Foundation of China (82300068, 82303294, 82302395 and 82102227), the Fundamental Research Funds for the Central Universities (2024CDJXY017), the Natural Science Foundation of Shanghai (22YF1437400), the Young Elite Scientists Sponsorship Program by CAST (2023QNRC001), and the Natural Science Foundation of Chongqing (cstc2021jcyj-msmX0529).

Appendix A. Supplementary data

Supplementary data to this article can be found online at https://doi.org/10.1016/j.mtbio.2024.101208.

References

[1] Y. Xu, D. Li, Z. Yin, A. He, M. Lin, G. Jiang, X. Song, X. Hu, Y. Liu, J. Wang, X. Wang, L. Duan, G. Zhou, Tissue-engineered trachea regeneration using decellularized trachea matrix treated with laser micropore technique, Acta Biomater. 58 (2017) 113–121.

[2] D. Fabre, F. Kolb, E. Fadel, O. Mercier, S. Mussot, T. Le Chevalier, P. Dartevelle, Successful tracheal replacement in humans using autologous tissues: an 8-year experience, Ann. Thorac. Surg. 96 (4) (2013) 1146–1155.

[3] B. Xie, W. He, D. Xie, G. Jiang, A novel technique to increase the length of tracheal resection by adding an autologous pedicled pectoralis major myocutaneous flap transposition, Ann. Thorac. Surg. 98 (6) (2014) 2236–2238.

[4] P. Delaere, J. Vranckx, G. Verleden, P. De Leyn, D. Van Raemdonck, Tracheal allotransplantation after withdrawal of immunosuppressive therapy, N. Engl. J. Med. 362 (2) (2010) 138–145.

[5] E.M. Genden, B.A. Miles, T.J. Harkin, S. DeMaria, A.J. Kaufman, E. Mayland, V. F. Kaul, S.S. Florman, Single-stage long-segment tracheal transplantation, Am. J. Transplant. 21 (10) (2021) 3421–3427.

[6] J.F. Azorin, F. Bertin, E. Martinod, M. Laskar, Tracheal replacement with an aortic autograft, Eur. J. Cardio. Thorac. Surg. 29 (2) (2006) 261–263.

[7] E. Martinod, K. Chouahnia, D.M. Radu, P. Joudiou, Y. Uzunhan, M. Bensidhoum, A. M. Santos Portela, P. Guiraudet, M. Peretti, M.-D. Destable, A. Solis, S. Benachi, A. Fialaire-Legendre, H. Rouard, T. Collon, J. Piquet, S. Leroy, N. Vénissac, J. Santini, C. Tresallet, H. Dutau, G. Sebbane, Y. Cohen, S. Beloucif, A. C. d'Audiffret, H. Petite, D. Valeyre, A. Carpentier, E. Vicaut, Feasibility of bioengineered tracheal and bronchial reconstruction using stented aortic matrices, JAMA 319 (21) (2018) 2212–2222.

[8] Y. Xu, J. Dai, X. Zhu, R. Cao, N. Song, M. Liu, X. Liu, J. Zhu, F. Pan, L. Qin, G. Jiang, H. Wang, Y. Yang, Biomimetic trachea engineering via a modular ring strategy based on bone-marrow stem cells and atelocollagen for use in extensive tracheal reconstruction, Adv. Mater. 34 (6) (2022) e2106755.

[9] S. Kawaguchi, T. Nakamura, Y. Shimizu, T. Masuda, T. Takigawa, Y. Liu, H. Ueda, T. Sekine, K. Matsumoto, Mechanical properties of artificial tracheas composed of a mesh cylinder and a spiral stent, Biomaterials 22 (23) (2001) 3085–3090.

[10] J.F. Weber, S.S. Rehmani, M.Z. Baig, Y. Jadoon, F.Y. Bhora, Successes and failures in tracheal bioengineering: lessons learned, Ann. Thorac. Surg. 112 (4) (2021) 1089–1094.

[11] J. Schneppendahl, S. Thelen, S. Twehues, C. Eichler, M. Betsch, J. Windolf, M. Hakimi, M. Wild, The use of biodegradable sutures for the fixation of tibial eminence fractures in children: a comparison using PDS II, Vicryl and FiberWire, J. Pediatr. Orthop. 33 (4) (2013) 409–414.

[12] D.H. Kim, J.B. Lee, M.L. Kang, J.H. Park, J. You, S. Yu, J.Y. Park, S.B. Ryu, G. M. Seon, J.K. Yoon, M.H. Lee, Y.M. Shin, K.D. Park, J.C. Park, W.S. Jang, W.S. Kim, H.J. Sung, Microneedle vascular couplers with heparin-immobilized surface improve suture-free anastomosis performance, ACS Biomater. Sci. Eng. 4 (11) (2018) 3848–3853.

[13] W. Gao, K. Chen, W. He, S. Zhao, D. Cui, C. Tao, Y. Xu, X. Xiao, Q. Feng, H. Xia, Synergistic chondrogenesis promotion and arthroscopic articular cartilage restoration via injectable dual-drug-loaded sulfated hyaluronic acid hydrogel for stem cell therapy, Compos. B Eng. 263 (2023) 110857.

[14] Z. Huang, Y. Zhang, R. Liu, Y. Li, M. Rafique, A.C. Midgley, Y. Wan, H. Yan, J. Si, T. Wang, C. Chen, P. Wang, M. Shafiq, J. Li, L. Zhao, D. Kong, K. Wang, Cobalt loaded electrospun poly(epsilon-caprolactone) grafts promote antibacterial activity and vascular regeneration in a diabetic rat model, Biomaterials 291 (2022) 121901.

[15] H.M. Zhang, M. Guo, T.H. Zhu, H. Xiong, L.M. Zhu, A careob-like nanofibers with a sustained drug release profile for promoting skin wound repair and inhibiting hypertrophic scar, Compos Part B-Eng 236 (2022) 109790.

[16] M. Rafique, T. Wei, Q. Sun, A.C. Midgley, Z. Huang, T. Wang, M. Shafiq, D. Zhi, J. Si, H. Yan, D. Kong, K. Wang, The effect of hypoxia-mimicking responses on improving the regeneration of artificial vascular grafts, Biomaterials 271 (2021) 120746.

[17] H. Yan, Q. Cheng, J. Si, S. Wang, Y. Wan, X. Kong, T. Wang, W. Zheng, M. Rafique, X. Li, J. He, A.C. Midgley, Y. Zhu, K. Wang, D. Kong, Functionalization of in vivo tissue-engineered living biotubes enhance patency and endothelization without the requirement of systemic anticoagulant administration, Bioact. Mater. 26 (2023) 292–305.

[18] Y. Zhang, K. Xu, D. Zhi, M. Qian, K. Liu, Q. Shuai, Z. Qin, J. Xie, K. Wang, J. Yang, Improving vascular regeneration performance of electrospun poly(ε-caprolactone) vascular grafts via synergistic functionalization with VE-cadherin/VEGF, Advanced Fiber Materials 4 (6) (2022) 1685–1702.

[19] E.R. Gao, Y. Wang, P.L. Wang, Q.Y. Wang, Y.X. Wei, D.Y. Song, H.F. Xu, J.H. Ding, Y. Xu, H.T. Xia, R. Chen, L. Duan, C-shaped cartilage development using wharton's jelly-derived hydrogels to assemble a highly biomimetic neotrachea for use in circumferential tracheal reconstruction, Adv. Funct. Mater. 33 (14) (2023).

[20] X. Wang, F. Li, L. Xie, J. Crane, G. Zhen, Y. Mishina, R. Deng, B. Gao, H. Chen, S. Liu, P. Yang, M. Gao, M. Tu, Y. Wang, M. Wan, C. Fan, X. Cao, Inhibition of overactive TGF-β attenuates progression of heterotopic ossification in mice, Nat. Commun. 9 (1) (2018) 551.

[21] G. Liu, Q. Guo, C. Liu, J. Bai, H. Wang, J. Li, D. Liu, Q. Yu, J. Shi, C. Liu, C. Zhu, B. Li, H. Zhang, Cytomodulin-10 modified GelMA hydrogel with kartogenin for in-situ osteochondral regeneration, Acta Biomater. 169 (2023) 317–333.

[22] L. Wang, L. Lin, H. Qi, J. Chen, P. Grossfeld, Endothelial loss of ETS1 impairs coronary vascular development and leads to ventricular non-compaction, Circ. Res. 131 (5) (2022) 371–387.

[23] E. Music, T.J. Klein, W.B. Lott, M.R. Doran, Transforming growth factor-beta stimulates human bone marrow-derived mesenchymal stem/stromal cell chondrogenesis more so than kartogenin, Sci. Rep. 10 (1) (2020) 8340.

[24] T. Nishida, S. Kubota, E. Aoyama, M. Takigawa, Impaired glycolytic metabolism causes chondrocyte hypertrophy-like changes via promotion of phospho-Smad1/5/8 translocation into nucleus, Osteoarthritis Cartilage 21 (5) (2013) 700–709.

[25] M. Hou, Y. Zhang, X. Zhou, T. Liu, H. Yang, X. Chen, F. He, X. Zhu, Kartogenin prevents cartilage degradation and alleviates osteoarthritis progression in mice via the miR-146a/NRF2 axis, Cell Death Dis. 12 (5) (2021) 483.

[26] V. Lefebvre, M. Angelozzi, A. Haseeb, SOX9 in cartilage development and disease, Curr. Opin. Cell Biol. 61 (2019) 39–47.

[27] D.G. O'Shea, T. Hodgkinson, C.M. Curtin, F.J. O'Brien, An injectable and 3D printable pro-chondrogenic hyaluronic acid and collagen type II composite hydrogel for the repair of articular cartilage defects, Biofabrication 16 (1) (2023).

[28] Z.W. Hao, T.H. Chen, Y. Wang, Q.Y. Feng, J.Y. Chen, H.K. Li, J.W. Wang, Z. P. Wang, Z.Y. Zhang, R.X. Chen, G. Shi, Z.W. Zou, L. Cai, T.H. Zhu, J.F. Li, Self-assembling peptide nanofibers anchored parathyroid hormone derivative for bone tissue engineering, Advanced Fiber Materials 6 (2) (2024) 583–606.

[29] Y.H. Liu, L.R. Wang, Z. Liu, Y.H. Kang, T.H. Chen, C. Xu, T.H. Zhu, Durable immunomodulatory nanofiber niche for the functional remodeling of cardiovascular tissue, ACS Nano 18 (1) (2023) 951–971.

[30] Y. Xu, Y.F. Guo, Y.Q. Li, Y.Y. Huo, Y.L. She, H. Li, Z.H. Jia, G.N. Jiang, G.D. Zhou, Z.W. You, L. Duan, Biomimetic trachea regeneration using a modular ring strategy based on poly(sebacoyl diglyceride)/polycaprolactone for segmental trachea defect repair, Adv. Funct. Mater. 30 (42) (2020).

[31] D. Xia, D. Jin, Q. Wang, M. Gao, J. Zhang, H. Zhang, J. Bai, B. Feng, M. Chen, Y. Huang, Y. Zhong, N. Witman, W. Wang, Z. Xu, H. Zhang, M. Yin, W. Fu, Tissue-engineered trachea from a 3D-printed scaffold enhances whole-segment tracheal repair in a goat model, Journal of tissue engineering and regenerative medicine 13 (4) (2019) 694–703.

[32] Y. Xu, H. Duan, Y.Q. Li, Y.L. She, J.J. Zhu, G.D. Zhou, G.N. Jiang, Y. Yang, Nanofibrillar decellularized wharton's jelly matrix for segmental tracheal repair, Adv. Funct. Mater. 30 (14) (2020).

[33] E.M. Boazak, D.T. Auguste, Trachea mechanics for tissue engineering design, ACS Biomater. Sci. Eng. 4 (4) (2018) 1272–1284.

[34] J.C. Shelton, D.L. Bader, D.A. Lee, Mechanical conditioning influences the metabolic response of cell-seeded constructs, Cells Tissues Organs 175 (3) (2003) 140–150.

[35] J. Villalba-Caloca, A. Sotres-Vega, D.M. Giraldo-Gómez, M.O. Gaxiola-Gaxiola, M. C. Piña-Barba, J.A. García-Montes, S. Martínez-Fonseca, M. Alonso-Gómez, J. A. Santibáñez-Salgado, In vivo performance of decellularized tracheal grafts in the reconstruction of long length tracheal defects: experimental study, Int. J. Artif. Organs 44 (10) (2021) 718–726.

[36] J.A. Felix, M.L. Woodruff, E.R. Dirksen, Stretch increases inositol 1,4,5-trisphosphate concentration in airway epithelial cells, Am. J. Respir. Cell Mol. Biol. 14 (3) (1996) 296–301.

[37] B. Ressler, R.T. Lee, S.H. Randell, J.M. Drazen, R.D. Kamm, Molecular responses of rat tracheal epithelial cells to transmembrane pressure, Am. J. Physiol. Lung Cell Mol. Physiol. 278 (6) (2000) L1264–L1272.

[38] T. Georgiev-Hristov, M. García-Arranz, I. García-Gómez, M.A. García-Cabezas, J. Trébol, L. Vega-Clemente, P. Díaz-Agero, D. García-Olmo, Sutures enriched with adipose-derived stem cells decrease the local acute inflammation after tracheal anastomosis in a murine model, Eur. J. Cardio. Thorac. Surg. 42 (3) (2012) e40–e47.

[39] Y. Watanabe, S. Sasada, T. Izumo, Y. Nakamura, C. Chavez, S. Watanabe, T. Tsuchida, Intractable obstructive endobronchial granulation caused by surgical materials after sleeve resection for tracheal carcinoma, Ann. Thorac. Surg. 98 (6) (2014) 2200–2202.

[40] C.D. Wright, H.C. Grillo, J.C. Wain, D.R. Wong, D.M. Donahue, H.A. Gaissert, D. J. Mathisen, Anastomotic complications after tracheal resection: prognostic factors and management, J. Thorac. Cardiovasc. Surg. 128 (5) (2004) 731–739.